Applied Catalysis B: Environmental 182 (2016) 504–512

Contents lists available at ScienceDirect

Applied Catalysis B: Environmental

journal homepage: www.elsevier.com/locate/apcatb

Biomolecule-assisted self-assembly of CdS/MoS_2/graphene hollow spheres as high-efficiency photocatalysts for hydrogen evolution without noble metals

Xuelian Yu[a], Ruifeng Du[a], Baoying Li[a], Yihe Zhang[a,*], Huijuan Liu[b], Jiuhui Qu[b], Xiaoqiang An[b,**]

[a] Beijing Key Laboratory of Materials Utilization of Nonmetallic Minerals and Solid Wastes, National Laboratory of Mineral Materials, School of Materials Science and Technology, China University of Geosciences, 100083 Beijing, China
[b] Key Laboratory of Drinking Water Science and Technology, Research Center for Eco-Environmental Sciences, Chinese Academy of Sciences, Beijing 100085, China

ARTICLE INFO

Article history:
Received 29 June 2015
Received in revised form 1 September 2015
Accepted 2 September 2015
Available online 7 September 2015

Keyword:
Graphene
Photocatalytic hydrogen evolution
Molybdenum disulfide
Biomolecules
Hollow spheres

ABSTRACT

Despite the great potential of hollow nanomaterials for energy applications, most approaches rely on hard template-based multistep process for tailoring the interior structure, while the template-free self-assembly synthesis still remains challenging. In this work, we developed a facile biomolecule-assisted one-pot strategy toward the fabrication of novel CdS/MoS_2/graphene hollow spheres. The molecular structure of cysteine was found to be crucial for controlling the morphology of composites. Due to the unique hollow-shaped structure and improved charge separation ability, CdS/5 wt% MoS_2/2 wt% graphene hollow spheres exhibited superior high activity for visible-light-driven water splitting without noble metals. The synergistic effects of graphene and MoS_2 on the photocatalytic hydrogen production were further investigated by time-resolved fluorescence, electrochemical impedance and Mott–Schottky measurements. This method opens promising prospects for the rational design of high-efficiency and low-cost photocatalysts for hydrogen evolution based on graphene and MoS_2.

1. Introduction

Photocatalytic water splitting to produce hydrogen using solar energy has been a focus of great attention as a possible means for converting solar energy to chemical energy in the form of clean and renewable hydrogen fuel [1]. Up to now, a large number of semiconductor photocatalysts have been developed for hydrogen evolution, but several fundamental issues must be addressed before their industrial applications. One of the most challenging things is finding out more effective strategies to improve the efficiency. Graphene, a 2-D sheet of sp2-hybridized carbon, has attracted a lot of attention, due to the promising applications in the fields of flexible electronics, photovoltaics, sensing as well as photocatalysis. The good optical transmittance, large theoretical specific surface area and high intrinsic electron mobility make it an ideal platform to improve the efficiency of photocatalytic reactions [2,3]. To date, various graphene-based composites have been developed and applied in environmental remediation, water splitting, CO_2 photoreduction, etc. [4–6] However, most of these research focuses on the loading of semiconductor nanoparticles onto graphene sheets, the rational design of graphene-based photocatalytic composites with novel morphologies should be emphasized, as the photocatalytic activity strongly depends on the morphology and structure of photocatalysts [7–10].

Hollow structured nanomaterials have attracted special interest in recent years, owing to their unique physical and chemical properties and promising applications in nanoscale chemical reactors, encapsulation or controlled release of bioactive agents [11,12]. In particular, the large surface area and good permeability of hollow nanostructures can increase the active sites and light utilization by multiscattering of incidence light, which makes them ideal candidate for high-efficiency photocatalysts [13,14]. Therefore, it is attractive to develop hollow graphene-based photocatalysts, due to the synchronously combined characteristics of large surface area and high conductivity. However, hard template-assisted methods are generally used to fabricate hollow structured photocatalysts, the one-pot synthesis in a facile way is still a great

* Corresponding author.
** Corresponding author.
E-mail addresses: zyh@cugb.edu.cn (Y. Zhang), xqan@rcees.ac.cn (X. An).

http://dx.doi.org/10.1016/j.apcatb.2015.09.003
0926-3373/

challenge to material scientists. Biomolecule-assisted synthesis has been proven to be a novel, environment-friendly and promising method in the preparation of nanomaterials owing to its convenience and unique advantages in morphology control. Cysteine, an amino acid normally as a building block of proteins that are used throughout the body, has been successfully used to construct metal sulfide nanosheets/graphene composites with desired shapes and significantly improved interfacial contact for charge separation [15,16]. Thereafter, investigation of the effects of these biomolecules on the development of novel hollow nanomaterials is of great importance, which would offer great opportunities to fabricate high-performance graphene-based photocatalysts for hydrogen production.

Another consideration of the present hydrogen production photocatalysts is their dependence on the expensive noble metals (such as Pt, Ru and Rh), which are generally used as co-catalysts to retard the recombination of electron-hole pairs. Due to their high cost, it is valuable to develop highly efficient and noble-metal free photocatalysts to further facilitate the development of hydrogen evolution [17,18]. MoS_2, a typical layered transition metal sulfide, has been proved to be a promising catalyst for the hydrogen evolution reaction (HER) [19–22]. Due to the existence of active edge sites, recent reports indicate that nano-sized MoS_2 is showing promise as a low-cost cocatalyst for water activation to produce hydrogen, with comparable activity to Pt [23–27]. Although several strategies have been developed to fabricate MoS_2 loaded photocatalysts for hydrogen evolution, the synthesis procedures are usually complicated, as involving multi-step reactions [28,29]. To the best of our knowledge, the synthesis of hollow structured MoS_2-loaded photocatalysts through facile one-pot reaction has been seldom studied. Furthermore, the expected synergistic effects between MoS_2 co-catalysts and conductive graphene sheets may provide new concepts for the design of high-efficiency photocatalysts [30].

Inspired by these concepts, CdS, a typical II-VI group semiconductor, was chosen as model photocatalyst to construct CdS/MoS_2/graphene hollow nanomaterials. It was found that L-cysteine could not only act as sulfur source for the simultaneous formation of CdS and MoS_2, its structural transformation under alkaline situation also plays an important role in the self-assembly of graphene skeleton for the formation of CdS/MoS_2/graphene hollow spheres. Due to the unique hollow-shaped structure and enhanced charge separation ability, CdS/MoS_2/graphene hollow spheres exhibited superior activity for visible-light-driven photocatalytic hydrogen production. We believe this facile one-pot method will open promising prospects for utilizing environmental-friendly biomolecules to develop high-efficiency and low-cost photocatalysts with controlled morphologies and structures.

2. Experimental

2.1. Synthesis of CdS/MoS_2/graphene composites

Graphene oxide (GO) solution was synthesized from natural graphite powder by a modified Hummers' method. CdS/MoS_2/graphene hybrids with different ratios of graphene and MoS_2 were fabricated through the one-step hydrothermal reaction. Firstly, $Cd(OAc)_2$ (0.266 g) was added to DI water (30 mL) with calculated amount of GO solution (1 wt%, 2 wt% and 3 wt% of CdS). After the ultrasonic treatment for 0.5 h, cysteine (0.24 g) and a certain amount of sodium molybdate (1 wt%, 3 wt%, 5 wt% and 7 wt% of CdS) were added into the solution under vigorous stirring. After stirring for 2 h, the homogeneous solution was transferred into a Teflon-lined autoclave and held at 200 °C for 24 h. Then, the product was cooled to room temperature, separated by centrifugation and washed with water for five times. Pure CdS nanoparticles was synthesized through the same procedure, except for the addition of GO and sodium molybdate.

2.2. Characterization

X-ray diffraction (XRD) patterns were recorded using a Bruker D8 Advance diffractometer with high-intensity Cu Kα1 irradiation (λ = 1.5406 Å). The morphologies of the products were characterized by field-emission scanning electron microscope (FESEM, FEI, Quanta 400 FEG), transmission electron microscopy (TEM, Philips, CM120). The structure and composition of product is determined by high-resolution transmission electron microscopy (HRTEM, FEI, TecnaiF20) equipped with Energy Dispersive Spectrometer (EDS, Oxford, INCA X-Act). Gold-coated TEM grids from Ted-Pella were used as substrates. Raman spectroscopy was carried out using laser micro-Raman spectrometer (Horiba Jobin Yvon T64000). The XPS data were determined on an AXIS Ultra instrument (Kratos, UK). The photoluminescence spectra (PL) were investigated on a fluorometry (F-4500, Hitachi). The time-resolved fluorescence spectra were measured by a F900 fluorescence spectrometer with excitation at 375 nm.

2.3. Fabrication of film electrodes and electrochemical measurements

5 mg of composite and Nafion solution (5 wt%) (10 μL) were dispersed in 1 mL water/isopropanol mixed solvent (3:1 v/v) by at least 30 min sonication to form a homogeneous catalyst colloid. Then 5 μL of the catalyst colloid was loaded onto the surface of a pre-polished glassy carbon (GC) disk electrode (3 mm in diameter) and left to dry in air at room temperature.

Electrochemical measurements were performed on a ZAHNER ZENNIUM electrochemical workstation (ZAHNER Instrument, Inc.). Platinum wire and saturated calomel electrode (SCE) were used as counter and reference electrode, respectively. The prepared thin film GC electrode was used as working electrode. The electrochemical impedance spectra (EIS) measurement was performed in the presence of a 2.5 mM $K_3[Fe(CN)_6]/K_4[Fe(CN)_6]$ (1: 1) mixture as a redox probe in 0.1 M KCl solution. The impedance spectra were recorded with the help of Z_{Plot}/Z_{View} software under an AC perturbation signal of 5 mV over the frequency range of 1 MHz to 100 mHz. Mott–Schottky measurement was carried out from −-1 V to −0.5 V in a solution containing 0.5 M Na_2SO_4.

2.4. Photocatalytic activity measurements

The photocatalytic H_2 production experiments were carried out in a Pyrex reaction cell connected to a closed gas circulation with an evacuation system. In a typical experiment, 30 mg of the prepared photocatalysts were dispersed in a 50 mL mixed solution of lactic acid (5 mL) and water (45 mL). Prior to irradiation, the suspension was purged with argon to remove dissolved air. Then, the system was irradiated by a 300 W xenon lamp with a 400 nm cut-off filter. The amount of hydrogen was analyzed by a gas chromatograph (Varian GC-450, TCD and 5 Å molecular sieve column). For the contrast measurements, samples were uniformly platinized and photodeposited 1% Pt by photoreduction of H_2PtCl_6 aqueous solution.

3. Results and discussion

The morphology and composition of CdS/MoS_2/graphene composite are studied in Fig. 1. As shown in Fig. 1a, typical spherical-like structures with the diameter of 600–900 nm are obviously seen in the composite. From the broken spheres and partial collapsed shells, these spheres have a clear hollow interior voids with holes

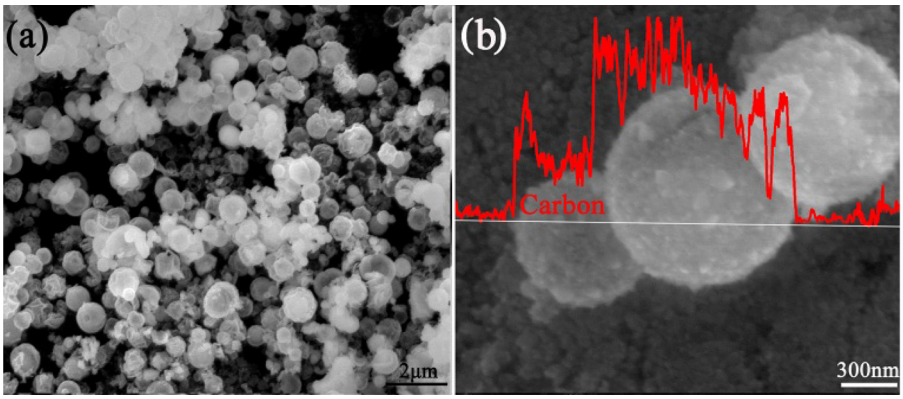

Fig. 1. (a) SEM image of CdS/MoS_2/graphene hollow spheres. (b) Line scan profile of C element in CdS/MoS_2/graphene hollow spheres.

on the surfaces. The elemental composition of hollow spheres can be confirmed by the EDS spectrum in Fig. S1. Except the signal of Au originated from the Au grid, carbon, molybdenum, sulfur and cadmium elements are detected in the composite. Fig. 1b is the line scan profile of C element in the CdS/MoS_2/graphene hollow spheres. It can be clearly seen that with the scanning going rightward, the signal of C is significantly increased. Reaching the margin of hollow spheres, the sharp drop of signal is easily observed. This is a clear evidence for the distribution of graphene layer as 3-D skeleton of hollow spheres.

The structure of a single CdS/MoS_2/graphene hollow sphere is further characterized by HRTEM. Fig. 2a is the TEM image of CdS/MoS_2/graphene hollow spheres, the dark edge and pale center of product further confirms the typical hollow interior structure. The thickness of the coarse shell is estimated to be about 80 nm. It can be seen from Fig. 2b that the shell of the hollow sphere is composed of loosely packed nanoparticles, with the diameter of about 30 nm. The nanoparticles are uniformly embedded into transparent wrinkled nanosheets, indicating the formation of graphene wrapped hollow spheres (Fig. S3). To support this, CdS/MoS_2 composites were also fabricated and the morphology characterizations are shown in Fig. S4. Generally, the absence of graphene exhibits ignorable effects on the formation of hollowed structures. Differently, shells of CdS/MoS_2 hollow spheres are composed only of small nanoparticles. Graphene with wrinkled sheet-like structures is not observed at the edge of spheres. The high-resolution TEM image of nanoparticle in Fig. 2c shows a well-defined crystallinity of CdS with a lattice spacing of 0.36 nm, which is assigned to the (1 0 0) planes of hexagonal CdS. Notably, the surface of CdS nanoparticles are intimately coupled with layered hexagonal MoS_2 with an interlayer distance of 0.62 nm. Besides, lattice fringes can also be observed on the surface of graphene in Fig. 2d, which correspond to the (0 0 2) planes of MoS_2. Such hollow structure and intimate connection among CdS, MoS_2 and graphene is supposed to have more active sites for hydrogen evolution reaction.

Fig. S2 shows the XRD patterns of the CdS/MoS_2/graphene composite. Compared with pure CdS with a wurtzite structure (JCPDS Card No. 80-0006), the CdS/MoS_2/graphene composite shows similar diffraction pattern, excepting the appearance of the weak diffraction peak at $2\theta = 33^\circ$. This peak can be unambiguously assigned to the (1 0 0) plane of hexagonal MoS_2 (JCPDS Card No. 37-1492). Due to the low amount and relatively low diffraction intensity of graphene, no typical diffraction peaks of carbon species are observed in the composite, which is similar as the literature reports [31]. Raman spectroscopy measurement is carried out to investigate the chemical structures of hollow spheres. In Fig. S5, the three strong peaks around 293 cm^{-1}, 588 cm^{-1} and 886 cm^{-1} can be ascribed to the longitudinal optical (LO) phonons of CdS nanoparticles [32]. Another two peaks at 1338 cm^{-1} and 1588 cm^{-1}, corresponding to the D and G bands of graphene, indicate the concurrent existence of graphene in the composites.

XPS is further used to study the valence state of elements in the composites. As shown in Fig. 3a, the overall XPS spectrum of CdS/MoS_2/graphene hollow spheres shows typical signals of carbon, molybdenum, sulfur, cadmium and neglectable oxygen. Fig. 3b is the C1s spectrum of CdS/MoS_2/graphene hollow spheres, which can be deconvoluted into three peaks. The binding energies located at 284.6, 287.7 and 288.9 eV are due to the graphitic sp2 carbon (C—C), carbonyls (C═O) and carboxyl (O—C═O) functional groups respectively [33]. The relative content of carbon in the sample is estimated to confirm the degree of reduction. The deoxygenation of grapheme oxide (GO) in hollow spheres is well confirmed by the higher content of graphitic sp2 carbon (80.1%) than that of GO (41.9%), indicating the formation of graphene in the composite. [34] The binding energies of Cd 3d doublet are located at 405.1 eV and 411.9 eV (Fig. 3c), consist with the values reported in the literature for Cd^{2+} in CdS. In Fig. 3d, the high-resolution XPS in the Mo 3d range of the composite shows a peak at 225.1 eV corresponding to the S 2s binding energy of CdS and MoS_2. The double peaks for Mo 3d are found at 231.9and 227.8 eV, indicating the reduction of Mo^{6+} to Mo^{4+} and the formation of MoS_2 in the composite. Compared to the reported results, a slight shift of binding energy is detected, which can be ascribed to the strong interactions between MoS_2 and the other components. [35] Therefore, all of the above results indicate the formation of CdS/MoS_2/graphene hollow spheres.

To find out the possible formation mechanism of hollow spheres, the influence of experimental condition on the morphology of product is investigated. In the absence of GO and sodium molybdate, only solid CdS nanoparticles of ~60 nm are obtained (Fig. 4a). As shown in Fig. 4b, the addition of GO shows no effect on the formation of hollow structure. Differently, the morphology of products is significantly influenced by the introduction of sodium molybdate. For CdS/1 wt% MoS_2/graphene composite in Fig. 4c, spherical aggregates with the diameter of 500 nm are distinctly observed, which are tightly wrapped by graphene. Both solid spheres and hollow spheres with typical hollow interior voids can be observed, when the percentage of MoS_2 increases to 3 wt% (Fig. 4d). In Fig. 4e, the sample with 7 wt% MoS_2 shows the same hollow morphology as CdS/5 wt% MoS_2/graphene composites (the image shown in Fig. 1). Furthermore, MoS_2/graphene composites are shown in Fig. 5f, which consist of ultrathin 2D nanosheets, when CdS is totally replaced by MoS_2. These results indicate that moderate amount of sodium molybdate is critical for the formation of graphene wrapped CdS/MoS_2 hollow spheres.

Based on the above discussion, a possible growth mechanism of CdS/MoS_2/graphene hollow spheres is proposed (Scheme 1). With

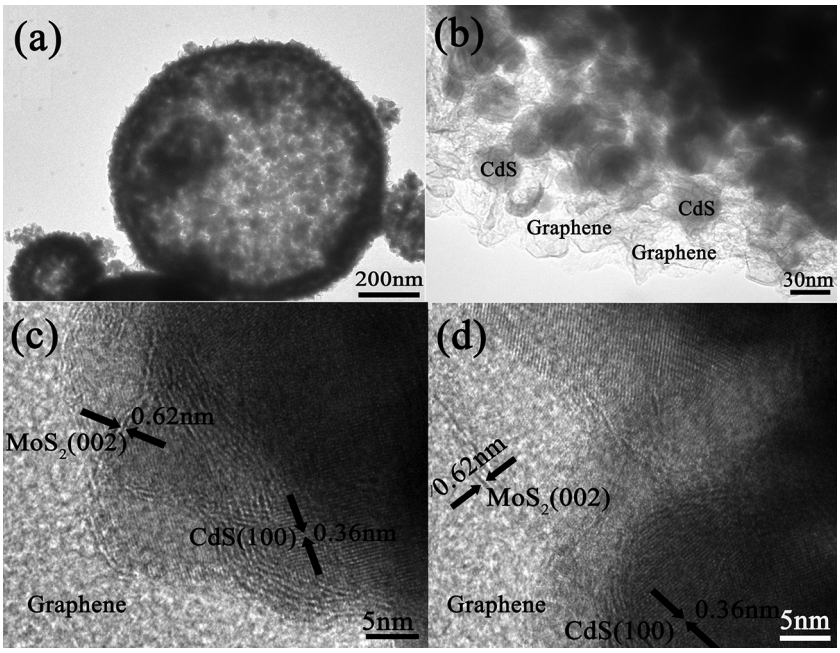

Fig. 2. (a–b) TEM images of CdS/MoS_2/graphene hollow sphere, (c–d) HRTEM images of CdS/MoS_2/graphene hollow sphere.

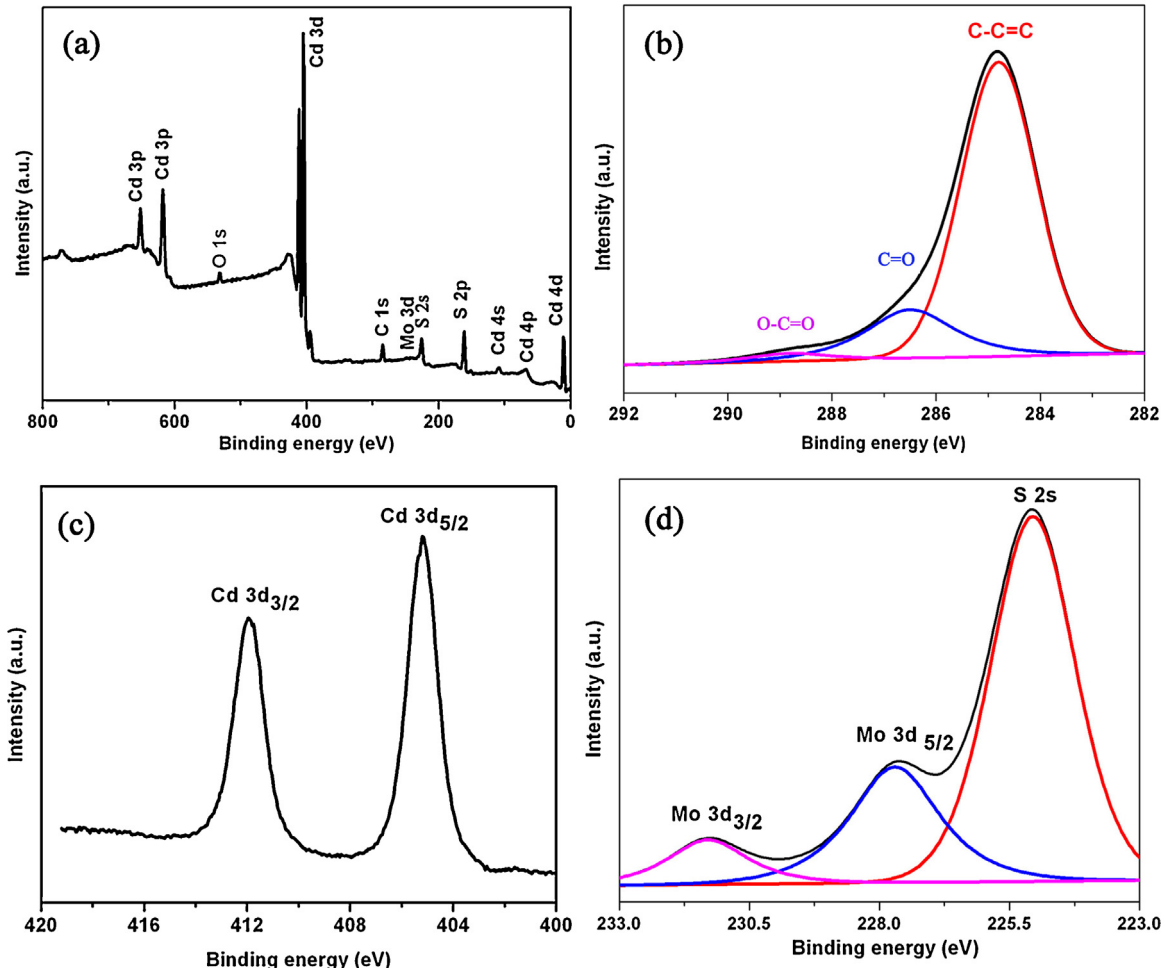

Fig. 3. (a) Full XPS spectrum of CdS/MoS_2/graphene hollow spheres and the peak deconvolution of the (b) C 1s, (c) Cd 3d, and (d) Mo 3d spectra.

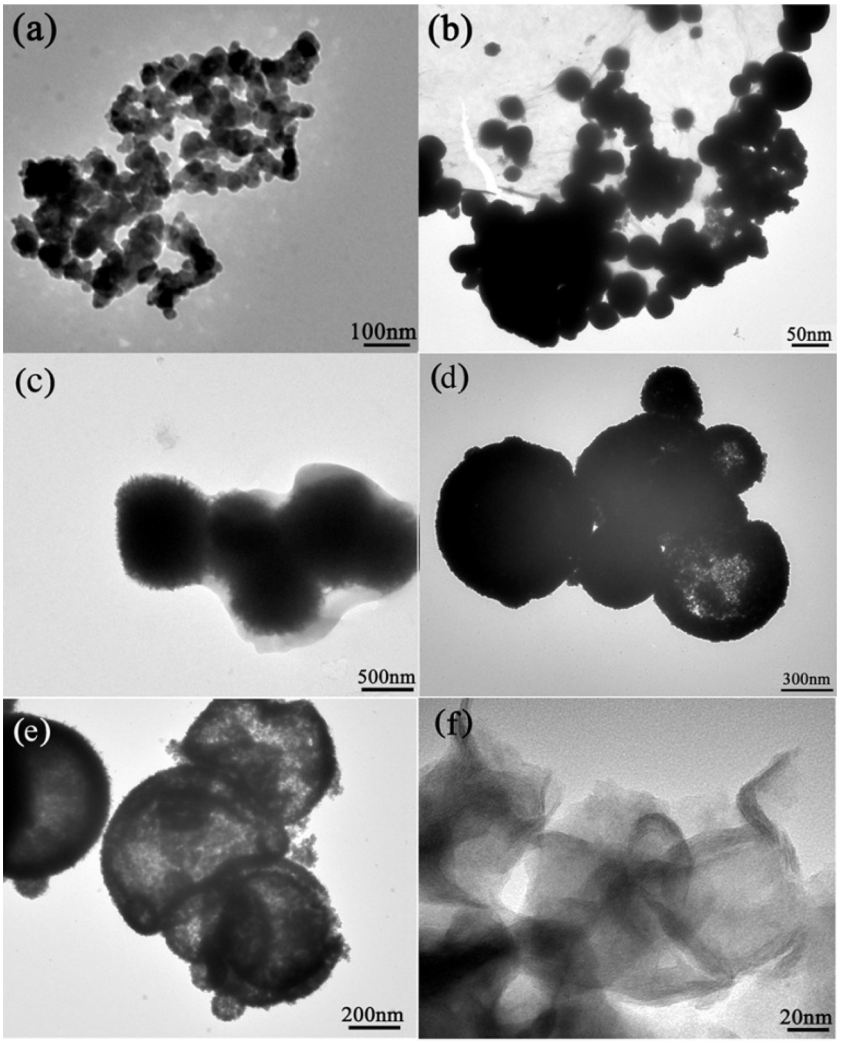

Fig. 4. TEM images of (a) CdS nanoparticles, (b) CdS/graphene composites, (c) CdS/1 wt% MoS_2/2 wt% graphene composites, (d) CdS/3 wt% MoS_2/2 wt% graphene composites, (e) CdS/7 wt% MoS_2/2 wt% graphene composites, (f) MoS_2/graphene nanosheets.

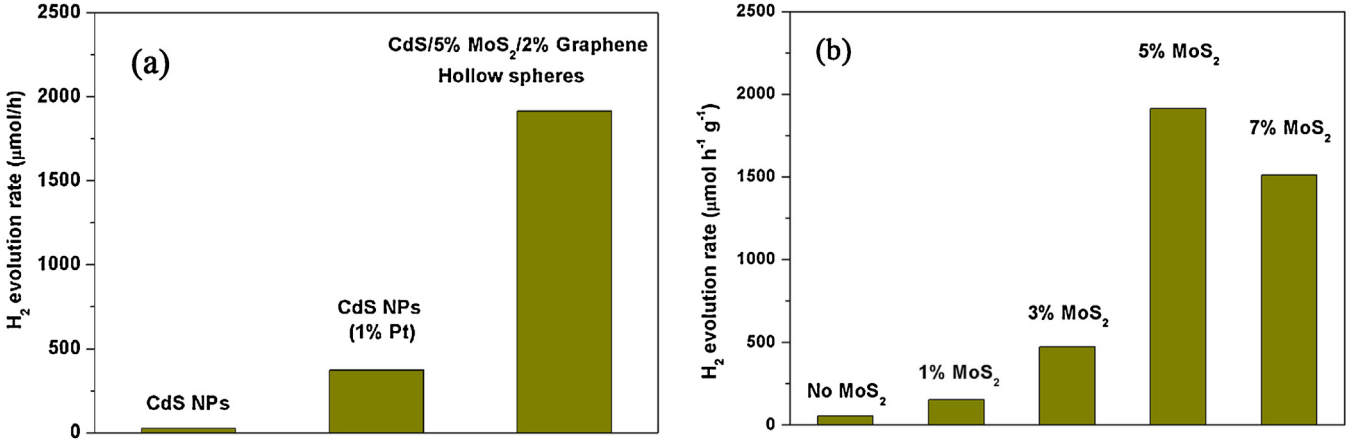

Fig. 5. Hydrogen evolution based on (a) pure CdS and CdS/5% MoS_2/2% graphene hollow spheres, (b) CdS/MoS_2/graphene composites with different contents of MoS_2.

multifunctional groups (such as -NH_2, -COOH, and -SH), cysteine can be used as a complexing agent and structure directing molecule, through the conjugation with metal ions or other functional groups [36]. In Step I, Cd (Mo)-cysteine complexes are formed because of the interaction between Cd (Mo) precursors and cysteine. [37] In Step II, Cd (Mo)-cysteine complexes are self-assembled into sphere-shaped particles through the attachment of complex with abundant uncoordinated groups. Similar phenomenon has already been observed during the fabrication of metal-cysteine nanostructures, as we found that the self-assembly of complex into hollow

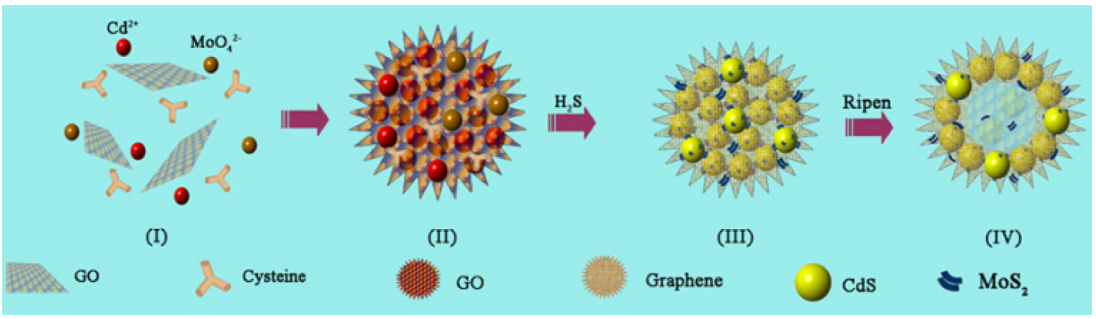

Scheme 1. Schematic illustration of the growth mechanism of CdS/MoS_2/graphene hollow spheres.

spheres could be controlled by the amount of alkaline additives (monoethanolamine). [38] Here, sodium molybdate plays a dual role as precursor of MoS_2 and weakly alkaline additive, which is a crucial factor for the biomolecule-assisted self-assembly of hollow spheres [39]. Meanwhile, the surface of GO is usually negatively charged in this case. The sites of carboxyl, epoxide and hydroxyl groups show strong affinity to the uncoordinated groups, which results in the hybridization of graphene in the spherical complex [40]. In Step III, the complexes are slowly pyrolysed, resulting in the formation of cadmium (molybdenum) sulfide nuclei on GO. Meanwhile, the released H_2S acts not only as a sulfur source for the nucleation of semiconductor nanocrystals, but also as a reductant for the restoration of sp2 conjugated structures in graphene [41]. Under hydrothermal condition, the large surface energy of unstable nuclei would contribute to the dissolution and recrystallization of crystal nuclei. Due to the Ostwald ripening process and the generation of gas bubbles in Step IV, CdS/MoS_2/graphene hollow spheres formed. This cysteine-assisted self-assembly process is further validated by a control experiment. As can be seen from Fig. S6, the assembly of reaction precursors into spherical products was clearly observed, when kept the solution stirring for several days. It well confirms the strong interaction between precursors in the presence of cysteine.

The photocatalytic activity of products for H_2 production is evaluated under visible-light irradiation using lactic acid as a scavenger. As shown in Fig. 5a, the pure CdS nanoparticles show negligible activity (27 μmol h^{-1} g^{-1}) because of the fast recombination of electron–hole pairs. When 1 wt% Pt is used as co-catalyst, the photocatalytic H_2 production rate is increased to 373 μmol h^{-1} g^{-1}. Interestingly, CdS/5 wt% MoS_2/2 wt% graphene hollow spheres show a remarkable H_2 production rate of 1913 μmol h^{-1} g^{-1}, even without utilizing any noble metal as co-catalyst. It proves the impacts of hollow structured nanomaterials as well as the synergetic effects of MoS_2 and graphene on the photocatalytic activities of CdS for H_2 production. In the control experiments, the effects of fabrication conditions on the performance of photocatalysts are investigated. Firstly, the content of MoS_2 in the composites exhibits significant effect on the activities, as shown in Fig. 5b. With the increase of the content of MoS_2, the photocatalytic activities increase first and achieve the highest hydrogen yield in the presence of 5% MoS_2. The further increase of MoS_2 content to 7% leads to a slightly deteriorated performance. Fig. S3 presents the results of hydrogen evolution over 5% MoS_2 loaded photocatalysts, with different content of graphene. The introduction of graphene shows beneficial effect on the photocatalytic reaction, following the order of CdS/MoS_2/2 wt% graphene>CdS/MoS_2/3 wt% graphene>CdS/MoS_2/1 wt% graphene. Although hollow structured photocatalysts can also be fabricated based on the biomolecule-assisted strategy, the hydrogen evolution rate over CdS/MoS_2 hollow spheres is only 672 μmol h^{-1} g^{-1}. It agrees well with the fact that the charge recombination can be significantly suppressed in the graphene incorporated composites. Furthermore, much lower photocatalytic activity is achieved over the physical mixture of CdS, MoS_2 and graphene. It indicates that the synergetic effects around heterostructured interfaces are crucial for the improvement of photocatalytic performance.

To illustrate the enhanced photocatalytic activity of CdS/MoS_2/graphene hollow spheres, photoluminescence (PL) emission spectra is used to investigate the efficiency of charge carrier trapping, immigration and transfer. As shown in Fig. 6a, well-resolved peak at 524 nm is observed in the spectrum of pure CdS nanoparticles, which can be attributed to the radiative recombination of photogenerated electrons and holes. Differently, strong fluorescence quenching is observed in the spectrum of CdS/MoS_2/graphene hollow spheres. To understand the lifetime of charge carriers in the composites, the luminescence decay measurements are studied in Fig. 6b. Compared with pure CdS nanoparticles, the PL lifetime of CdS/MoS_2/graphene hollow

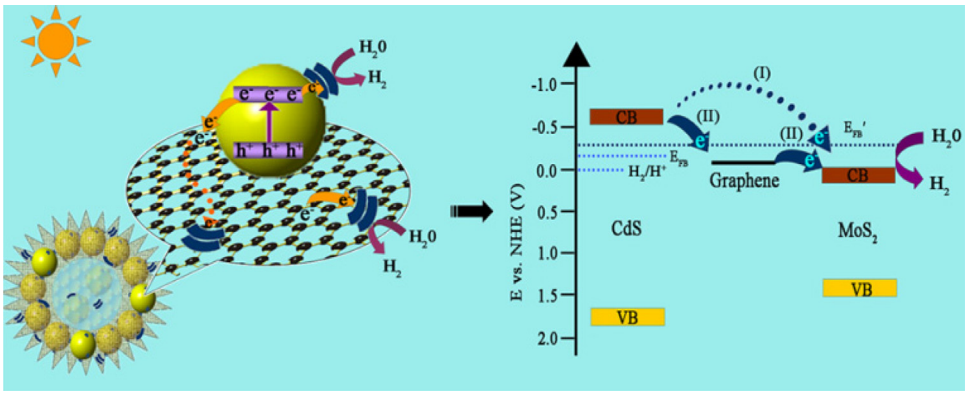

Scheme 2. Schematic diagram of the charge transfer in the CdS/MoS_2/graphene hollow spheres under visible light irradiation.

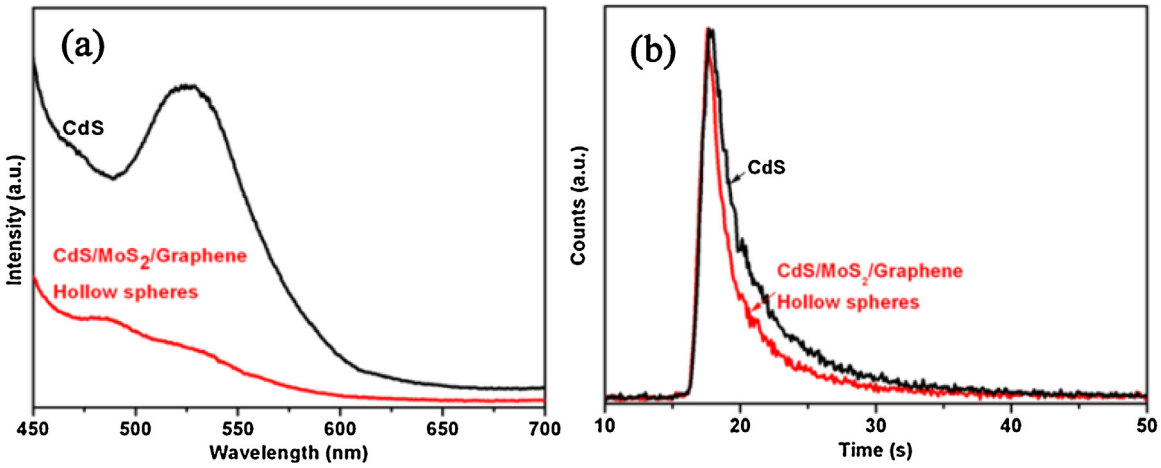

Fig. 6. (a) Photoluminescence spectra of CdS nanoparticles and CdS/MoS_2/graphene hollow spheres. (b) Time-resolved fluorescence decays of CdS nanoparticles and CdS/MoS_2/graphene hollow spheres.

spheres is remarkably shortened from 7.2 ns to 5.9 ns. The fluorescence quenching and shortened PL lifetime indicate that graphene can efficiently separate and transport photoinduced electrons. [42] Thus, the suppressed recombination of charge carriers is one reason for the improved photocatalytic activity of CdS/MoS_2/graphene hollow spheres.

Electrochemical impedance spectra (EIS) measurement is an effective tool to study the charge transfer at the semiconductor/electrolyte interface. As can be seen in Fig. 7a, the Nyquist spectrum of CdS/MoS_2/graphene hollow spheres shows a much smaller radius than that of pure CdS nanoparticles. It indicates that the transport of charge carriers is indeed significantly influenced by the hybridization of graphene into semiconductor [43]. Obviously, the spectrum of CdS/MoS_2/graphene hollow spheres shows two semicircles. The radius of these arcs is easily distinguished from the magnified image in Fig. 7b. Based on the suggested equivalent model shown in the inset of Fig. 7a, the high-frequency intercept on the real axis represents the ohmic series resistance (R_s), corresponding to the bulk resistance of the electrolyte and electrodes. The first semicircle at the high frequency can be ascribed to the resistance (R_1) and chemical capacitance (CPE_1) of the solid-state interface layer formed in the passivation reaction. The second semicircle at medium frequency corresponds to the charge transfer resistance (R_2) and double layer capacitance (CPE_2). Furthermore, Warburg impedance (W) originated from the diffusion of ions on the surface of electrodes can also be observed at the low frequency region. [44] Compared to pure CdS nanoparticles, the much smaller internal impedances (i.e., R_s, R_1, and R_2) of CdS/MoS_2/graphene hollow spheres indicate the decreasing of solid state interface layer resistance and charge transfer resistance [45]. Therefore, it is believed that the role of graphene as both electron acceptor and transporter contribute to the effective separation and transfer of photogenerated charge carriers in the hollow spheres.

Mott–Schottky analysis is used to determine both donor density and flat band potential (E_{FB}) at semiconductor/liquid interface. In Fig. 8a, the positive slopes clearly indicate the *n*-type semiconductor properties of both pure CdS nanoparticles and CdS/MoS_2/graphene hollow spheres. The higher carrier concentration in hollow spheres is reasonably deduced from the much lower slope of the linear region. It is believed that the increased donor density can efficiently improve the charge transport in CdS and the interfacial electron transfer. Therefore, the shift of Fermi level toward the conduction band of CdS is theoretically expected [46].

As we know, to achieve overall photocatalytic water splitting, the bottom level of the conduction band should be more negative than the reduction potential of H^+/H_2 (0 V vs NHE at PH = 0) [47]. For *n*-type semiconductor, it is well known that the flat band potential (E_{FB}) measured according to Mott–Schottky is close to the conduction band of semiconductor. [48] As shown in Fig. 8b, E_{FB} of CdS/MoS_2/graphene hollow spheres is −0.99 V vs. SCE, calculated from the x intercepts of the linear region. Compared to the value of −0.88 V for pure CdS, the negative shift of 0.11 V is observed. Generally, E_{FB} varies as a function of pH value and can be quantified by the equation $E_h = 0 - 0.059 \times pH$. As the pH of electrolyte is about 7, the calculated hydrogen evolution potential of pure CdS nanoparticles and CdS/MoS_2/graphene hollow spheres are −0.225 and −0.317 V vs. NHE (pH0) respectively. [49] The upward shift of E_{FB} indicates the higher band bending and the more efficient charge transfer at the solid/liquid interface. [50] With more negative energy level than the reduction potential of H^+/H_2, the hydrogen evolution reaction over the CdS/MoS_2/graphene hollow spheres is facilitated. Furthermore, two distinct pseudo Mott–Schottky slopes are observed in the composites, indicating the formation of surface states around heterostructured interfaces, which agrees well with the XPS results [51].

Based on the above results, the superior photocatalytic activity of CdS/MoS_2/graphene hollow spheres for Pt-free hydrogen production can be ascribed to the following reasons:

(1) The unique hollow structure of composite shows impact on the H_2 production activity. On one hand, the void interiors structure of CdS/MoS_2/graphene hollow spheres can provide more active sites and allow multiple reflections of visible light within the interior cavities. On the other hand, 2D graphene with high specific surface area offers perfect substrate for photocatalytic reaction, which is critical for high-efficiency photocatalysts.
(2) With lower activation potentials and more active sites for H_2 production, MoS_2 has been reported to be a promising co-catalyst to replace expensive noble metals. During the one-pot reaction, the formed CdS/MoS_2 heterojunction will show better contact because of the in-situ growth of MoS_2. Therefore, more photogenerated electrons in CdS can efficiently transfer to MoS_2 layers and react with H^+ to form H_2 under much lower overpotential (Step I in Scheme 2).
(3) As shown in Scheme 2, the role of graphene as both electron acceptor and charge transporter is crucial for the superior activity of the synergic system. Firstly, the charge recombination in

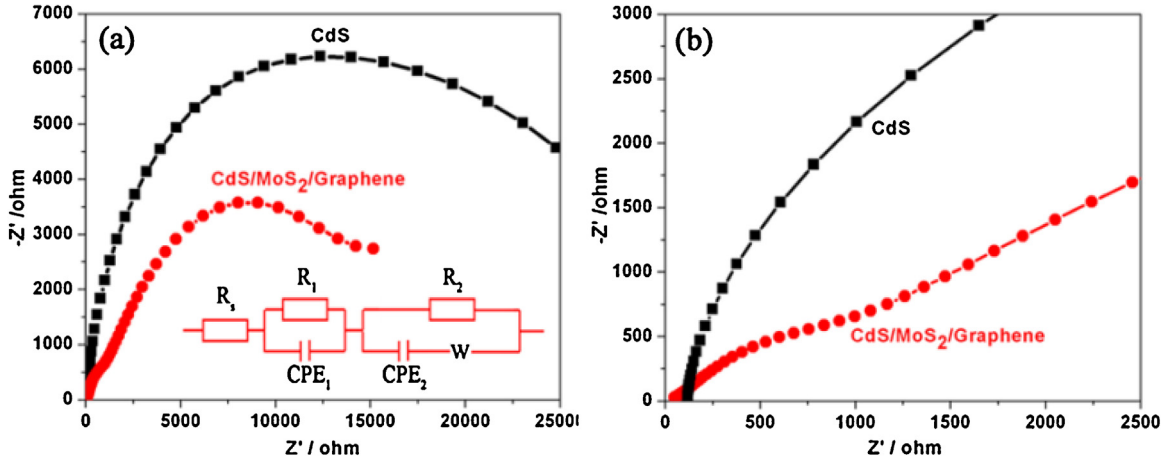

Fig. 7. (a) Electrochemical impedance spectra (EIS) of CdS nanoparticles and CdS/MoS_2/graphene hollow spheres modified electrodes. The inset shows an equivalent circuit for the electrodes. (b) Magnified image of Nyquist plots.

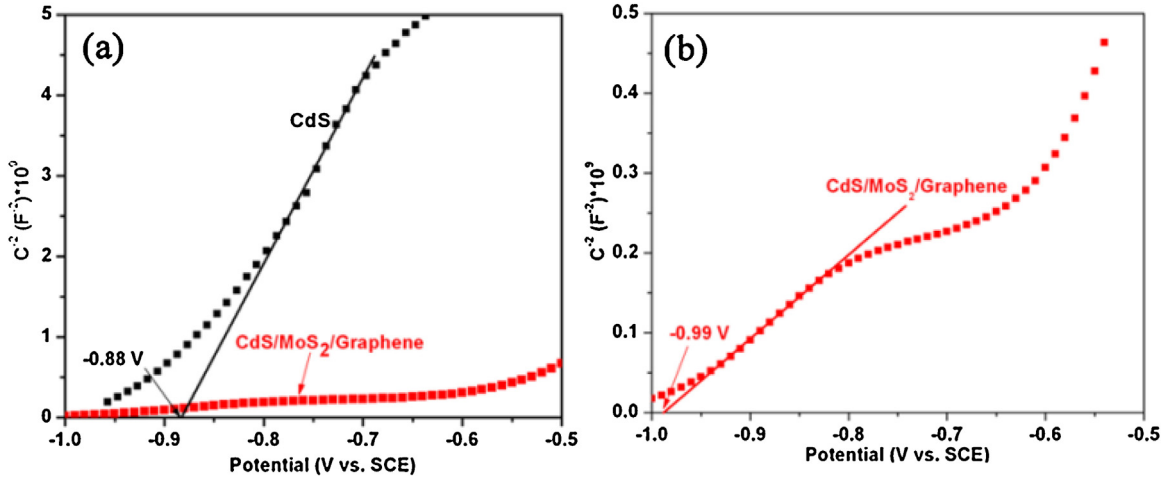

Fig. 8. (a) Mott–Schottky plots of CdS nanoparticles and CdS/MoS_2/graphene hollow spheres. (b) Magnified image of Mott–Schottky plots of CdS/MoS_2/graphene hollow spheres.

CdS is greatly inhibited because of the existence of graphene with high conductivity. Secondly, the stepwise electron transfer process is expected because of the intermediate energy level of graphene in the composites (Step II in Scheme 2). Undoubtedly, the multifunction of graphene as novel photocatalytic mat facilitates the fully use of photogenerated electrons, which remarkably enhances the activity of CdS/MoS_2/graphene hollow spheres.

(4) As shown in Scheme 2, the upward shift of E_{FB} to E_{FB}'results in the higher band bending at the solid/liquid interface. Therefore, the more efficient charge transfer contributes to the high electron mobility and donor density, which is benefit for photocatalytic H_2 production.

4. Conclusion

In summary, a facial one-pot self-assembly process was used to fabricate CdS/MoS_2/graphene hollow spheres for high-efficiency photocatalytic hydrogen evolution reaction. Based on the fluorescence and electrochemical measurements, the superior photocatalytic activity of CdS/MoS_2/graphene hollow spheres is ascribed to the large surface area of hollow structure, inhibited charge recombination and the synergetic electron transfer on the photocatalyst mat. Therefore, this kind of noble-metal-free CdS/MoS_2/graphene hollow spheres has great potential for photocatalytic H_2 production under visible light irradiation.

Acknowledgments

This work was supported by the National Natural Science Foundation of China (Grant 21401212, 51578531), Fundamental Research Funds for the Central Universities (2652015086).

Appendix A. Supplementary data

Additional structural characterizations and photocatalytic activities of products. Supplementary data associated with this article can be found, in the online version, at http://dx.doi.org/10.1016/j.apcatb.2015.09.003.

References

[1] H. Tong, S.X. Ouyang, Y.P. Bi, N. Umezawa, M. Oshikiri, J.H. Ye, Adv. Mater. 24 (2012) 229–251.
[2] M. Yang, N. Zhang, M. Pagliaro, Y. Xu, Chem. Soc. Rev. 43 (2014) 8240–8254.
[3] L. Tan, W. Ong, S. Chai, A. Mohame, Appl. Catal. B Environ. 166–167 (2015) 251–259.
[4] G. Xie, K. Zhang, B. Guo, Q. Liu, L. Fang, J. Gong, Adv. Mater. 25 (2013) 3820–3839.
[5] X. An, J.C. Yu, RSC Adv. 1 (2011) 1426–1434.
[6] W. Tu, Y. Zhou, Z. Zou, Adv. Funct. Mater. 23 (2013) 4996–5008.

[7] Z.G. Yi, J.H. Ye, N. Kikugawa, T. Kako, S.X. Ouyang, H. Stuart-Williams, H. Yang, J.Y. Cao, W.J. Luo, Z.S. Li, Nat. Mater. 9 (2010) 559–564.
[8] X. Ouyang, H. Tong, N. Umezawa, J.Y. Cao, P. Li, Y.P. Bi, Y.J. Zhang, J.H. Ye, J. Am. Chem. Soc. 134 (2012) 1974–1977.
[9] S.B. Yang, Y.J. Gong, J.S. Zhang, L. Zhan, L.L. Ma, Z.Y. Fang, R. Vajtai, X.C. Wang, P.M. Ajayan, Adv. Mater. 25 (2013) 2452–2456.
[10] A. Iwase, Y.H. Ng, Y. Ishiguro, A. Kudo, R. Amal, J. Am. Chem. Soc. 133 (2011) 11054–11057.
[11] L. Shen, L. Yu, H. Wu, X. Yu, X. Zhang, X. Lou, Nat. Commun. 6 (2015) 6694.
[12] L. Shen, L. Yu, X. Yu, X. Zhang, X. Lou, Angew. Chem. Int. Ed. 54 (2015) 1868–1872.
[13] M. Luo, Y. Liu, J. Hu, H. Liu, J. Li, ACS Appl. Mater. Interfaces 4 (2012) 1813–1821.
[14] S. In, D. Vaughn II, R. Schaak, Angew. Chem. Int. Ed. 51 (2012) 3915–3918.
[15] Y. Zhao, L. Jiang, Adv. Mater. 21 (2009) 3621–3638.
[16] X. An, J.C. Yu, F. Wang, C. Li, Y. Li, Appl. Catal. B Environ. 129 (2013) 80–88.
[17] M. Nguyen, P.D. Tran, S.S. Pramana, R.L. Lee, S.K. Batabyal, N. Mathews, L.H. Wong, M. Graetzel, Nanoscale 5 (2013) 1479–1482.
[18] J. Zhang, J.G. Yu, M. Jaroniec, J.R. Gong, Nano Lett. 12 (2012) 4584–4589.
[19] D. Merki, X. Hu, Energy Environ. Sci. 4 (2011) 3878–3888.
[20] T. Jia, A. Kolpin, C. Ma, R. Chan, W. Kwok, S. Tsang, Chem. Commun. 50 (2014) 1185–1189.
[21] Q.H. Wang, K. Kalantar-Zadeh, A. Kis, J.N. Coleman, M.S. Strano, Nat. Nanotechnol. 7 (2012) 699–712.
[22] T.F. Jaramillo, K.P. Jorgensen, J. Bonde, J.H. Nielsen, S. Horch, I. Chorkendorff, Science 317 (2007) 100–102.
[23] C. Tsai, F. Abild-Pedersen, J. Norskov, Nano Lett. 14 (2014) 1381–1387.
[24] Y. Huang, R. Nielsen, W. Goddard, M. Soriaga, J. Am. Chem. Soc. 137 (2015) 6692–6698.
[25] X. Zong, H. Yan, G. Wu, G. Ma, F. Wen, L. Wang, C. Li, J. Am. Chem. Soc. 130 (2008) 7176–7177.
[26] X. Zong, G. Wu, H. Yan, G. Ma, J. Shi, F. Wen, L. Wang, C. Li, J. Phys. Chem. C 114 (2010) 1963–1968.
[27] H.I. Karunadasa, E. Montalvo, Y.J. Sun, M. Majda, J.R. Long, C.J. Chang, Science 335 (2012) 698–702.
[28] K. Chang, Z. Mei, T. Wang, Q. Kang, S. Ouyang, J. Ye, ACS Nano 8 (2014) 7078–7087.
[29] Q.J. Xiang, J.G. Yu, M. Jaroniec, J. Am. Chem. Soc. 134 (2012) 6575–6578.
[30] B. Hinnemann, P. Moses, J. Bonde, K. Jorgensen, J. Nielsen, S. Horch, I. Chorkendorff, J. Norskov, J. Am. Chem. Soc. 127 (2005) 5308–5309.
[31] H. Zhang, X. Lv, Y. Li, Y. Wang, J. Li, ACS Nano 1 (2010) 380–386.
[32] V. Dzhagan, M. Valakh, C. Himcinschi, A. Milekhin, D. Solonenko, N. Yeryukov, O. Raevskaya, O. Stroyuk, D. Zahn, J. Phys. Chem. C 118 (2014) 19492–19497.
[33] H. Li, S. Pang, S. Wu, X. Feng, K. Mullen, C. Bubeck, J. Am. Chem. Soc. 133 (2011) 9423–9429.
[34] X. An, J. Yu, Y. Wang, Y. Hu, X. Yu, G. Zhang, J. Mater. Chem. 22 (2012) 8525–8531.
[35] F. Meng, J. Li, S. Cushing, M. Zhi, N. Wu, J. Am. Chem. Soc. 135 (2013) 10286–10289.
[36] X. An, C. Cao, X. Yu, J. Nanosci. Nanotechnol. 10 (2010) 8356–8361.
[37] K. Chang, Z. Wang, G. Huang, H. Li, W. Chen, J. Lee, J. Power Sour. 201 (2012) 259–266.
[38] C. Cao, X. An, X. Yu, X. Ma, Curr. Nanosci. 6 (2010) 592–597.
[39] C. Cao, X. An, X. Yu, X. Ma, Curr. Nanosci. 6 (2010) 592–597.
[40] I. Kim, J. Lee, T. Kim, H. Kim, H. Kim, W. Choi, S. Hwang, Small 8 (2012) 1038–1048.
[41] D. Chen, L. Li, L. Guo, Nanotechnology 22 (2011) 325601.
[42] Y. Yang, W. Rodriguez-Coordoba, X. Xiang, T. Lian, Nano Lett. 12 (2012) 303–309.
[43] W. Jo, J. Jang, K. Kong, H. Kang, J. Kim, H. Jun, K. Parmar, J. Lee, Angew. Chem. Int. Ed. 51 (2012) 3147–3151.
[44] B. He, B. Dongand, H. Li, Electrochem. Commun. 9 (2007) 425–430.
[45] Y. Jang, X. Xin, M. Byun, Y. Jang, Z. Lin, D. Kim, Nano Lett. 12 (2012) 479–485.
[46] G. Wang, H. Wang, Y. Ling, Y. Tang, X. Yang, R. Fitzmorris, C. Wang, J. Zhangand, Y. Li, Nano Lett. 11 (2011) 3026–3033.
[47] X. Chen, S. Shen, L. Guo, S. Mao, Chem. Rev. 110 (2010) 6503–6570.
[48] Q. Xu, D. Wellia, Y. Ng, R. Amal, T. Tan, J. Phys. Chem. C 115 (2011) 7419–7428.
[49] W. Luo, Z. Li, X. Jiang, T. Yu, L. Liu, X. Chen, J. Ye, Z. Zou, Phys. Chem. Chem. Phys. 10 (2008) 6581–6717.
[50] Y. Qiu, K. Yan, H. Deng, S. Yang, Nano Lett. 12 (2012) 407–413.
[51] C. Zhen, L. Wang, L. Liu, G. Liu, G. Lu, H. Cheng, Chem. Commun. 49 (2013) 6191–6193.